at 311 nm under the same conditions. Therefore, the observed reaction traces for the acid-induced dissociation of NiA^+ and NiA_2 correspond to the dissociation of the 1:1 complex. The saturation-type behavior with respect to $[H^+]$ is consistent with the reaction mechanism shown in Figure 6. Krause et al.[16] have proposed a similar scheme to explain the reactions of Ca^{2+} and Mg^{2+} complexes of A23187 in 100% methanol. With use of the notation of the scheme in Figure 6, eq 15 may be written as in eq 20. The dissociation process occurs via parallel uncatalyzed

$$k_{obsd} = (k_d + k_H K_{NiAH}[H^+])/(1 + K_{NiAH}[H^+]) \quad (20)$$

(k_d) and proton-assisted ($K_{NiAH}k_H$) pathways. The resolved rate constant and equilibrium constant values are listed in Table III. The value obtained for k_d, combined with the value of k_{Ni}^A, derived from the formation rate experiments, gives a calculated value 7.55 for log K_{NiA}. This is in excellent agreement with the value of 7.54 obtained by fluorometric titration techniques.[11] The k_d value for Ni^{2+} may be compared with the analogous value obtained for Mg^{2+} in 70% methanol-water, 89 s^{-1},[16] and a preliminary value of ~ 30 s^{-1} in 80% methanol-water.[44] The values of k_{Mg}^A are 3.8×10^5 M^{-1} s^{-1} in 70% methanol-water and $\sim 1 \times 10^6$ M^{-1} s^{-1} in 65% methanol-water.[6] Therefore, the complexation selectivity of $\sim 2 \times 10^3$ (K_{NiA}/K_{MgA}) for Ni^+ over Mg^{2+} [16] is reflected primarily in the difference in the respective k_d values. The acid-assisted dissociation pathway involves rapid formation of a protonated Ni^{2+}-A23187 complex, $NiAH^{2+}$, which then undergoes first-order dissociation to the products, Ni^{2+} and HA. Similar behavior was reported for the Ca^{2+} and Mg^{2+} complexes of A23187 in 100% methanol[16] and for the acid-induced dissociation of sodium monensin in ethanol.[45] Furthermore, evidence for complexes of protonated monesin with monovalent cations in solution[46] and in the solid state[47] has been reported. The overall equilibrium constant, K', for the bottom reaction shown in Figure 6 is equivalent to $K_{H1}\gamma_H/K_{NiA}$, where γ_H is the activity coefficient for H^+ in 80% methanol-water. With use of the relationships

$$K' = k_{NiA}^H/k_{Ni}^{HA} = K_{NiAH}k_H/k_{Ni}^{HA} \quad (21)$$

and $\gamma_H = 0.64$ and the values listed in Table III, a value of 270 M^{-1} s^{-1} is calculated for k_{Ni}^{HA}. This is in good agreement with the somewhat imprecise value of 400 M^{-1} s^{-1} obtained from analysis of the formation kinetics. The initial site of proton attack may be the benzoxazole *N*-methylamino nitrogen, since this group is not involved in metal ion coordination. The proximity of the protonated amino group to the carboxylate carbonyl oxygen would facilitate an intramolecular proton transfer, thus enhancing the rate of nickel-carboxylate oxygen bond rupture.

The following observations may be made with regard to the complexation-dissociation kinetics of A23187. A23187 forms 1:1 complexes via parallel reactions of the anionic and protonated forms of the ionophore with the metal ion. The anionic form is much more reactive than the protonated form of the ionophore. Dissociation of the 1:1 and 1:2 Ni^{2+}-A23187 complexes in acidic medium occurs via parallel uncatalyzed and proton-assisted pathways. At pH* values greater than ~ 5.5, the acid-assisted pathway is negligible relative to the uncatalyzed (k_d) pathway. However, the effect of general acids, HX (i.e., CH_3COOH) is not yet known. The rates of formation seem to parallel the known solvent exchange rates of the cation for Mg^{2+} and Ni^{2+}, but the situation is not clear for more labile cations like Ca^{2+} [16] and Zn^{2+}. The high affinity of A23187 for the first-row transition-metal cations[11] coupled with the potentially slow dissociation rates may effect the Ca^{2+} transport rates at low ionophore concentrations.

Acknowledgment. This work was supported in part by U.S. Public Health Service Grant GM-24701 from the National Institutes of Health and by the University of Oklahoma Research Council.

(44) Thomas, T. P.; Taylor, R. W., unpublished result.
(45) Cox, B. G.; Firman, P.; Schneider, H. *J. Am. Chem. Soc.* **1985**, *107*, 4297-4300.
(46) Hoogerheide, J. G.; Popov, A. I. *J. Solution Chem.* **1979**, *8*, 83-95.
(47) Ward, D. L.; Wei, K. T.; Hoogerheide, J. G.; Popov, A. I. *Acta Crystallogr., Sect. B: Struct. Crystallogr. Cryst. Chem.* **1978**, *B34*, 110-115.
(48) Chapman, C. J.; Pfeiffer, D. R., unpublished result.
(49) Chaney, M. O.; Demarco, P. B.; Jones, N. D.; Occolowitz, J. L. *J. Am. Chem. Soc.* **1974**, *96*, 1932-1933.

Experimental Electron Density Distribution of Naloxone Hydrochloride Dihydrate, a Potent Opiate Antagonist

Cheryl L. Klein,[1a] Richard J. Majeste,[1b] and Edwin D. Stevens*[1c]

Contribution from the Department of Chemistry, Xavier University of Louisiana, New Orleans, Louisiana 70125, the Department of Chemistry, Southern University at New Orleans, New Orleans, Louisiana 70126, and the Department of Chemistry, University of New Orleans, New Orleans, Louisiana 70148. *Received September 2, 1986*

Abstract: The electron density distribution of naloxone hydrochloride dihydrate has been determined from high-resolution single-crystal X-ray diffraction measurements at 90 K. Intensities of 21 509 reflections were measured with Mo Kα radiation to a resolution of $((\sin\theta)/\lambda)_{max} = 1.0$ Å^{-1}. Averaging symmetry-related reflections yielded a set of 8573 independent reflections with an internal agreement factor of 2.7%. Least-squares refinement with a conventional spherical atom model converged at $R = 3.3\%$ and $R_w = 4.3\%$. Refinement with a multipole expansion model including parameters describing valence electron deformations yielded $R = 2.7\%$ and $R_w = 3.7\%$. Maps of the experimental electron density distribution have been calculated by using model structure factors from the multipole refinement. Proper treatment of the X-ray phases increases covalent bond peak heights by ca. 50% compared with electron density maps based on spherical atom phases. The experimental electron deformation density shows well-resolved peaks in all covalent bonds and two nonbonding peaks on the carbonyl oxygen. Only a single peak is observed for the nonbonding electrons on the furan oxygen, hydroxyl oxygens, and water molecules. Net atomic charges, obtained from X-ray monopole populations, are in qualitative agreement with charges derived from theoretical calculations. The concept of "local area charges" is introduced to minimize partitioning effects on the atomic charges. The nitrogen atom is found to have a negative net atomic charge of -0.52, despite the formal positive charge.

X-ray structure determination has long been an extremely powerful tool in attempts to derive quantitative structure-activity relationships of drugs and other biologically significant molecules. Accurate low-temperature X-ray measurements may be used,

0002-7863/87/1509-6675$01.50/0

Table I. Experimental Data

space group	$P2_12_12_1$ (acentric)
temp, K	90 (2)
cell dimensions	
a, Å	7.769 (3)
b, Å	13.202 (5)
c, Å	18.256 (7)
V, Å^3	1900.1
X-ray wavelength ($K\alpha_1$), Å	0.70930
d(calcd), g cm^{-3}	1.397
absorption coefficient, cm^{-1}	2.435
F(000)	848

however, to obtain not only structure but the experimental distribution of valence electrons as well.[2] Several studies on small molecules have demonstrated that such electron distributions obtained by X-ray diffraction are comparable in accuracy to large basis set ab initio theoretical calculations.[3] For molecules of moderate size (50–200 atoms) the experimental difficulties encountered increase only moderately with size, while the fourth-power dependence of ab initio calculations make theoretical calculations of similar accuracy on such molecules prohibitive.

In studies of drug–receptor interactions, it is reasonable to expect that, in addition to shape, the distribution of charge in a drug molecule will be of importance in receptor recognition and binding. Thus, high-resolution X-ray studies of drug molecules may yield significant new information.

To investigate the feasibility and potential usefulness of accurate electron density determinations, we have begun studies of a series of opiates including morphine (**1**), an agonist, and naloxone (**2**), a potent opiate antagonist. The ability of naloxone to displace

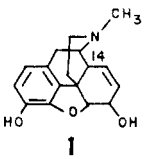

1

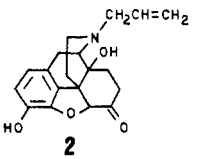

2

morphine and other agonists from the opiate receptor in competitive binding studies suggests a high degree of complementarity in both shape and charge with the receptor. Thus naloxone is useful in defining the shape and charge requirements of the receptor. In addition, unlike more flexible molecules which may also be active at the opiate receptor, the high degree of rigidity in the opiates, other than the *N*-alkyl group of naloxone, leaves little doubt as to the active conformation of the molecule.

By analysis of the experimental electron density distributions on a selected series of active opiates, the specific pattern of charge distribution necessary for optimum binding can be identified. Additionally, assuming the principle of receptor complementarity is valid for charge as well as shape, a three-dimensional model including both these factors may be constructed.

In addition to the implications for receptor binding, the experimental electron density distribution provides extremely detailed three-dimensional information on the electronic structure of the molecule itself. It can be used to determine experimental values for other one-electron properties of the molecule such as dipole moments, electrostatic potentials, and electric field gradients. The experimental density can therefore be used to correlate data obtained by other techniques, including approximate theoretical calculations. We report here the results of an experimental electron density mapping of naloxone hydrochloride dihydrate at low temperature.

Table II. Refinement Results

	I[c]	II[d]	III[e]	IV[f]
(sin θ)/λ range, Å^{-1}	0.0–1.0	0.6–1.0	0.0–1.0	0.0–1.0
N_{obsd}	6045	4176	6611	6608
N_v	348	140	756	313
R factors,[a] %				
R	3.3	3.3	2.7	3.7
R_w	4.3	4.1	3.7	4.9
GOF[b]	1.03	0.85	0.73	0.97

[a] $R = \sum||kF_o| - |F_c||/\sum|F_o|$ and $R_w = (\sum w(k|F_o| - |F_c|)^2/\sum wF_o^2)^{1/2}$. [b] "Goodness of fit" = $(\sum w(k|F_o| - |F_c|)^2/(N_{obsd} - N_v))^{1/2}$. [c] Full data refinement. [d] High-order refinement. [e] Multipole refinement. [f] Monopole refinement.

Experimental Section

Sample Preparation and Data Collection. Naloxone hydrochloride dihydrate was obtained from Sigma Chemical Co. and recrystallized from a dilute aqueous HCl solution. A large single crystal with approximate dimensions of 0.50 × 0.50 × 0.50 mm was mounted on an Enraf-Nonius CAD4 diffractometer and cooled to 90 ± 2 K with a stream of cold nitrogen gas using a locally modified Enraf-Nonius universal low-temperature device. Unit cell dimensions were obtained by least-squares refinement of 25 reflections with $36 \le 2\theta \le 44°$. Crystal data for naloxone hydrochloride dihydrate are summarized in Table I.

X-ray intensity measurements were collected in the ω–2θ scan mode with a graphite crystal monochromator and a molybdenum target X-ray tube. A total of 21 509 reflections were measured from three symmetry-equivalent octants to a 2θ maximum of 90° ((sin θ)/λ < 1.0 Å^{-1}). The data were corrected for Lorentz and polarization effects. Absorption as a function of ψ was observed to be minimal and was not corrected. Three standard reflections measured at 2-h intervals showed gradual fluctuations during data collection. Corrections to the intensity measurements and contributions to the esd's were calculated from polynomial fits to the observed behavior of the standards. Equivalent symmetry-related reflection intensities were averaged in order to lower the standard deviations in the measurements. The final data set gave 8573 independent reflections with an internal agreement factor[4] of R = 2.7%.

Least-Squares Refinements. The quantity $\sum w(k|F_o| - |F_c|)^2$ with $w = 1/\sigma(F)^2$ was minimized by full-matrix least-squares refinement. $\sigma^2(F^2)$ was taken as $[\sigma_{cs}^2 + (0.05)^2(F^2)^2 + (F^2)^2\sigma(k)^2]$, where σ_{cs} represents the contribution from counting statistics and $\sigma(k)$ is the contribution of the uncertainty in the scaling correction factor as determined by the fluctuations in the standard reflections.[5] Reflections where F_o was less than $3\sigma(F)$ were considered "observed" and were not included in the refinement. Computer programs used for data collection, reduction, and conventional refinement are part of the CAD4 SDP package.[6] Scattering factors were taken from ref 7 and included corrections for anomalous scattering contributions in the Cl, O, N, and C scattering factor tables. Initial fractional atomic coordinates for naloxone hydrochloride dihydrate were taken from a previously reported room-temperature structure determination.[8] Results of the conventional full data refinement can be found in Table II.

To reduce the bias in refined parameters from the aspherical features of the valence electron density, the parameters were refined with only high-angle data ((sin θ)/λ > 0.60 Å^{-1}) for which the scattering is due mainly to the core electrons. Hydrogen coordinates were obtained by extending the located hydrogen positions along the bond to positions yielding C–H, N–H, and O–H bond distances typical of values determined by neutron diffraction experiments. Results of this refinement (II) can be found in Table II.

An alternative technique for avoiding bias in the refined parameters is to include additional variables in the least-squares refinement which describe the aspherical features of the valence density.[9,10] In the model

(1) (a) Xavier University. (b) Southern University. (c) University of New Orleans.

(2) Coppens, P.; Stevens, E. D. *Adv. Quantum Chem.* **1977**, *10*, 1–35. Coppens, P.; Hall, M. *Electron Distributions and the Chemical Bond*; Plenum: New York, 1982. Angermund, K.; Claus, H. K.; Goddard, R.; Krüger, C. *Angew. Chem., Int. Ed. Engl.* **1985**, *24*, 237–356.

(3) Stevens, E. D. *Acta Crystallogr., Sect. B: Struct. Crystallogr. Cryst. Chem.* **1980**, *B36*, 1876–1886. Stevens, E. D.; Rys, J.; Coppens, P. *J. Am. Chem. Soc.* **1978**, *100*, 2324–2328. Stevens, E. D.; Rys, J.; Coppens, P. *Ibid.* **1977**, *99*, 265–267.

(4) Internal agreement factor: $R_I(F^2) = F_o^2 - \langle F_o^2\rangle/F_o^2$.

(5) McCandlish, L. E.; Stout, G. H.; Andrews, L. C. *Acta Crystallogr., Sect. A* **1975**, *A31*, 245–249.

(6) Frenz, B. *Computing in Crystallography*; Schenek, H., Olthholf-Hazekamp, R., van Koningsveld, H., Bassi, G. C., Eds.; Delft University Press: Delft, 1982.

(7) *International Tables for X-ray Crystallography*; Kynoch Press: Birmingham, England; 1974; Vol. 4.

(8) Karle, I. L. *Acta Crystallogr., Sect B: Struct. Crystallogr. Cryst. Chem.* **1974**, *B30*, 1682–1686.

(9) Dawson, B. *Proc. R. Soc. London, A*: **1967**, *298*, 255–263.

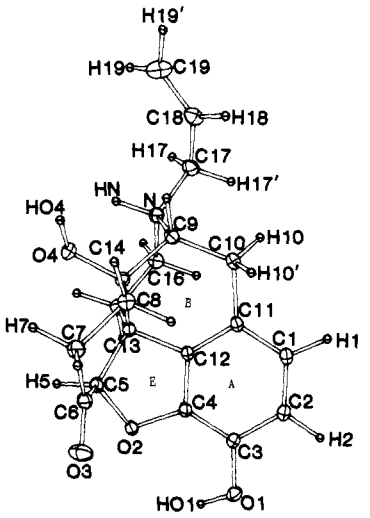

Figure 1. Molecular structure of naloxone hydrochloride at 90 K showing numbering system. Thermal ellipsoids are plotted at the 50% probability level.

used here, deformations of the electron density at each atom described by an expansion of multipole density functions

$$\rho_{\text{atom}} = \rho_c(r) + P_v\rho_v(\kappa' r) + \sum_{l,m} P_{l,m} R_l(\kappa'' r) y_{l,m}(\Theta,\Phi)$$

where ρ_c and ρ_v are spherical Hartree–Fock core and valence densities and $y_{l,m}$ are spherical harmonic functions in real form. The radial functions are given by

$$R_l(r) = N_l r^{n_l} e^{-\zeta_l r}$$

where n_l and ζ_l are chosen for each l as described previously.[10,11] The P_v, $P_{l,m}$, κ', and κ'' are refineable parameters. Positions and thermal parameters for hydrogens were obtained in the same manner as the high-order refinement and fixed at those values. Positional parameters for all atoms, anisotropic thermal parameters for non-hydrogen atoms, and multipole populations have been deposited as Supplementary Material.

Refinement IV is a monopole refinement including positional and thermal parameters of the non-hydrogen atoms and P_v and κ' for all atoms. Populations for the monopole functions, P_v, can be used to obtain net atomic charges for each of the atoms. These values can be found in Table III. Refinement results can be found in Table II.

Electron Density Maps. Distortions of the atomic electron distributions in a molecule as a result of chemical bonding are revealed in a plot of the deformation density, $\Delta\rho$, given as the difference between the total observed density and the density calculated for a superposition of spherical, neutral, Hartree–Fock atoms. Since the space group of naloxone hydrochloride dihydrate is acentric, the experimental $\Delta\rho_{HO}$ deformation densities suffer from the fact that only the amplitude, and not the phase, of the structure factor can be determined from the X-ray experiment. This has the effect of reducing the height and smearing out the features in the deformation density maps.[11-13] The maps presented here are model deformation density maps where the phases of the structure factors used to calculate the maps are those obtained from the multipole refinements.[11] On the basis of the errors in the X-ray measurements, the average standard deviation in the deformation density maps is estimated to be 0.05 e Å^{-3}. Close to atom centers, however, the errors will be higher because the deformation density is the difference between large values of the electron density.

A final difference map, or residual density, is calculated after the last cycle of the multipole refinement. The residual density is given as the difference between the total observed density and the density calculated from the multipole refinement parameters. This residual density is useful in judging the success of the model in fitting the significant features of the experimental electron density distribution.

(10) Hansen, N. K.; Coppens, P. *Acta Crystallogr., Sect. A: Found. Crystallogr.* **1978**, *A34*, 909–921.
(11) Stevens, E. D. *J. Am. Chem. Soc.* **1981**, *103*, 5087–5095.
(12) Savariault, J.-M.; Lehmann, M. S. *J. Am. Chem. Soc.* **1980**, *102*, 1298–1303.
(13) Klein, C. L.; Stevens, E. D. *Acta Crystallogr., Sect. B: Struct. Crystallogr. Cryst. Chem.* in press.

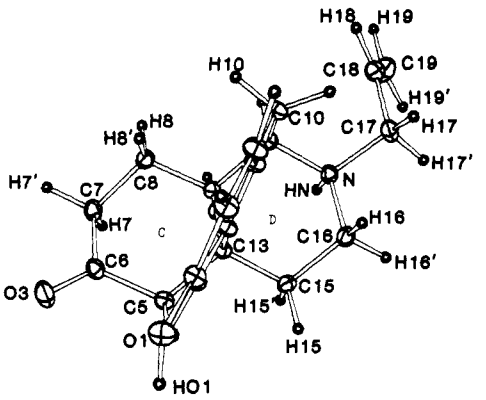

Figure 2. Molecular structure and numbering system for the face of the naloxone molecule perpendicular to that shown in Figure 1.

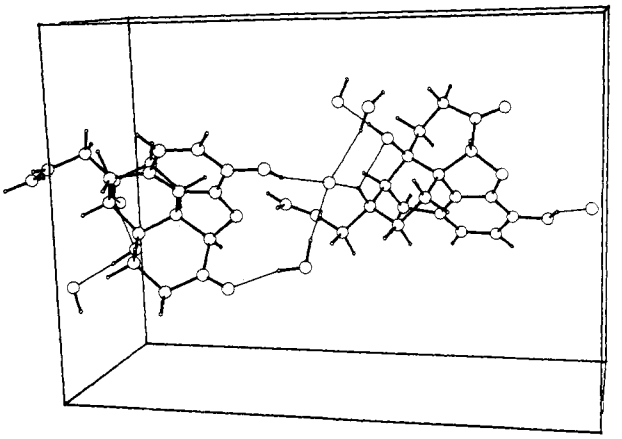

Figure 3. Plot of the hydrogen-bonding network in the structure of naloxone hydrochloride dihydrate at 90 K. Hydrogen bonds are indicated by thin lines.

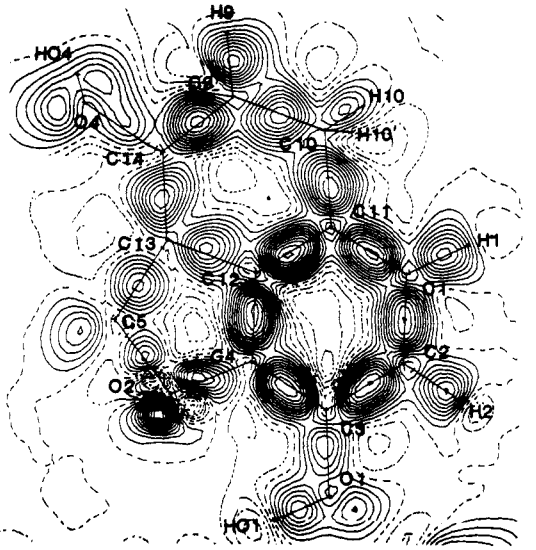

Figure 4. Experimental electron density distribution in naloxone hydrochloride dihydrate at 90 K. The map represents a composite of the dynamic model deformation density in the A, B, and E rings constructed by overlaying four individual maps calculated in planes which contain all of the ring atoms. Contours are calculated at 0.05 e Å^{-3} intervals with the zero and negative contours broken.

Results

The conformation of naloxone can be readily described as "T-shaped", similar to the geometries of other rigid opiates (i.e., morphine,[14,15] codeine,[16,17] and nalorphine[18]). In fact, rings A,

(14) Mackay, M.; Hodgkin, D. C. *J. Chem. Soc.* **1955**, 3261–3267.

Table III. Naloxone Hydrochloride Dihydrate Monopole Populations

atom	κ'	P_v	q	atom	κ'	P_v	q
Cl	0.979 (8)	7.64 (13)	−0.64				
O1	0.981 (6)	6.49 (7)	−0.49	HO1	1.58 (7)	0.40 (4)	0.60
O2	0.986 (8)	6.54 (9)	−0.54	HO4	1.58 (7)	0.59 (5)	0.41
O3	1.018 (9)	6.28 (8)	−0.28	HO5′	1.58 (7)	0.58 (5)	0.42
O4	0.981 (6)	6.82 (8)	−0.82	HO5″	1.58 (7)	0.56 (5)	0.44
O5	0.981 (7)	6.39 (9)	−0.39	HO6′	1.58 (7)	0.57 (5)	0.43
O6	0.981 (7)	6.59 (9)	−0.59	HO6″	1.58 (7)	0.37 (4)	0.63
N	0.990 (8)	5.52 (10)	−0.52	HN	1.36 (13)	0.60 (9)	0.40
C1	1.024 (8)	4.22 (9)	−0.22	HC1	1.27 (8)	0.74 (8)	0.26
C2	1.024 (8)	4.06 (9)	−0.06	HC2	1.27 (8)	0.70 (7)	0.30
C3	1.024 (8)	3.91 (8)	0.09	HC5	1.15 (2)	1.08 (6)	−0.08
C4	1.020 (8)	4.02 (10)	−0.02	HC7′	1.15 (2)	0.85 (5)	0.15
C5	1.014 (5)	3.78 (9)	0.22	HC7″	1.15 (2)	0.94 (6)	0.06
C6	1.016 (16)	3.92 (14)	0.08	HC8′	1.15 (2)	0.95 (6)	0.05
C7	1.014 (5)	4.20 (8)	−0.20	HC8″	1.15 (2)	0.91 (6)	0.09
C8	1.014 (5)	3.96 (8)	0.04	HC9	1.15 (2)	0.76 (5)	0.24
C9	1.014 (5)	4.49 (8)	−0.49	HC10′	1.15 (2)	0.58 (5)	0.42
C10	1.014 (5)	4.31 (9)	−0.31	HC10″	1.15 (2)	0.81 (5)	0.19
C11	1.020 (8)	4.04 (8)	−0.04	HC15′	1.15 (2)	0.69 (5)	0.31
C12	1.020 (8)	4.23 (9)	−0.23	HC15″	1.15 (2)	0.95 (5)	0.05
C13	1.014 (5)	4.22 (9)	−0.22	HC16′	1.15 (2)	0.81 (5)	0.19
C14	1.014 (5)	4.20 (8)	−0.20	HC16″	1.15 (2)	0.93 (5)	0.07
C15	1.014 (5)	4.26 (9)	−0.26	HC17′	1.15 (2)	0.96 (6)	0.04
C16	1.014 (5)	4.08 (10)	−0.08	HC17″	1.15 (2)	1.01 (5)	−0.01
C17	1.014 (5)	4.12 (10)	−0.12	HC18	1.32 (7)	0.86 (8)	0.14
C18	1.028 (11)	4.26 (11)	−0.26	HC19′	1.32 (7)	0.70 (7)	0.30
C19	1.028 (11)	3.95 (12)	0.05	HC19″	1.32 (7)	0.67 (7)	0.33

B, and E in naloxone and morphine are essentially identical with respect to corresponding bond lengths and angles.[8] ORTEP diagrams showing the structure and the numbering system of the faces of the "T" are shown in Figures 1 and 2. Specific structural characteristics for naloxone hydrochloride dihydrate have been described previously,[8] and no significant differences are observed in the present low-temperature study. The hydrogen-bonding network which includes the two water molecules and the chloride ion is shown in Figure 3.

Figure 4 shows the model deformation density map calculated through all of the atoms that describe rings A, B, and E. In the center of each bond in the molecule there are peaks of electron density corresponding to the redistribution of electron density that results from the sharing of electrons during covalent bond formation. On each of the atomic positions, there is little density or even a hole from where the atomic electron density had been subtracted. Dotted contours correspond to negative areas of electron density and solid contours correspond to positive areas of electron density. Since the face of naloxone shown in Figure 4 is not planar, the electron density distribution could not be plotted in one plane passing through all of the atoms. Instead, a different electron density map was calculated for the planar portions of the molecule, and these maps have been joined to give the composite electron density maps shown.

The deformation density in the two hydroxyl groups in naloxone (O1–HO1 and O4–HO4) can be seen in Figure 4. Both hydroxyl oxygen atoms show peaks of electron density corresponding to nonbonded lone pairs. The lone pairs have merged together into a single elongated peak with the maximum density in the plane plotted. This phenomenon has been observed in other hydroxyl oxygen atoms (i.e., oxalic acid[19]). The furan oxygen atom, O2, also shows the same elongated peak above and below the plane with the maximum in the center although the lone pair density on O2 appears to be much sharper than on the hydroxyl oxygen atoms. Figure 5 is a composite electron deformation density map

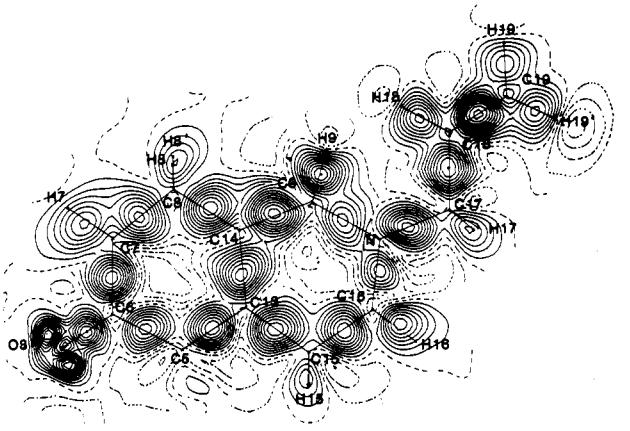

Figure 5. Experimental electron deformation density calculated through atoms of the C and D rings and the allyl group. Map constructed as in Figure 4 by overlaying nine planes. Contours plotted as in Figure 4.

for rings C and D and the allyl group. (This map was constructed by overlaying nine separate planes of density maps.) The lone pairs on the ketone oxygen, O3, are well resolved into two distinctive peaks of electron density. The C6=O3 bond peak shows additional buildup of electron density consistent with the "double-bond" character. Other areas of the molecule where there appears to be additional buildup of electron density are in the allyl group double bond and in the aromatic ring, as expected. One should notice also that the N–C and O–C bonds in naloxone appear to be lower in electron density than C–C bonds. The electron densities shown in the N–C bonds (Figure 5) and in the O–C bonds (Figure 4) suffer from the fact that the reference state of the molecule has more valence electrons that are subtracted from the total density when calculating the model deformation density maps. The result is N–C and O–C bonds that appear to have less electron density than C–C bonds.[19,21]

Figure 6 shows a model deformation density map calculated in the plane of the chloride ion showing the hydrogen bond network. The plane, defined by N, Cl, and O1, shows the electron

(15) Gylbert, L. *Acta Crystallogr., Sect. B: Struct. Crystallogr. Cryst. Chem.* **1973**, *B29*, 1630–1635.
(16) Lindsey, J. M.; Barnes, W. H. *Acta Crystallogr.* **1955**, *8*, 227–232.
(17) Kartha, G.; Ahmed, F. R.; Barnes, W. H. *Acta Crystallogr.* **1962**, *15*, 326–333.
(18) Duchamp, D. J.; Olson, E. C.; Chidester, C. G. *Am. Crystallogr. Assoc. Abstr., Ser. 2* **1977**, *5*, 83.
(19) Stevens, E. D.; Coppens, P. *Acta Crystallogr., Sect. B: Struct. Crystallogr. Cryst. Chem.* **1980**, *B36*, 1864–1876.
(20) Klein, C. L.; Stevens, E. D.; Zacharias, D. E.; Glusker, J. P. *Carcinogenesis* **1986**, *8*, 5–18.
(21) Dunitz, J. D.; Seiler, P. *J. Am. Chem. Soc.* **1983**, *105*, 7056–7058.

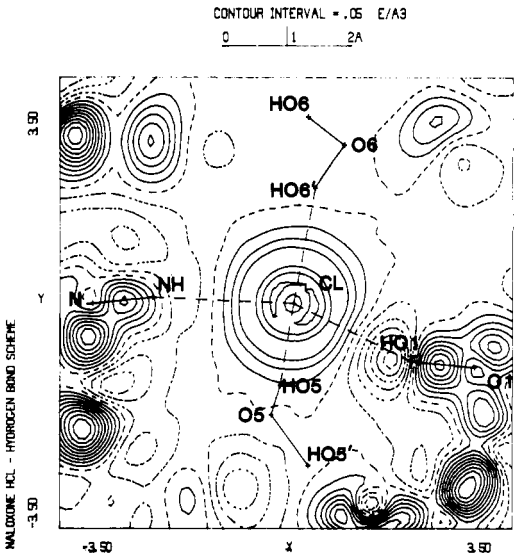

Figure 6. Experimental electron deformation density calculated in a plane defined by the Cl, N, and O1 atoms showing the hydrogen-bonding scheme and the deformation density in the N–H···Cl and O1–H···Cl hydrogen bonds. Contours plotted as in Figure 4.

Table IV

bond type	no. of contributions	av peak height, e Å^{-3} SA[a]	mult[b]	ratio
C(sp^2)–C(sp^2)	7	0.39 (4)	0.57 (5)	0.68
C(sp^3)–C(sp^3)	9	0.29 (5)	0.42 (6)	0.69
C(sp^2)–C(sp^3)	5	0.30 (7)	0.44 (7)	0.68
N–C(sp^3)	3	0.23 (6)	0.33 (10)	0.70
O–C	4	0.24 (3)	0.28 (5)	0.86
O=C	1	0.45	0.50	0.90
ketone lone pairs	2	0.35	0.60	0.58
furan lone pair	1	0.40	0.65	0.62
water lone pair	1	0.15	0.20	0.75

[a] Electron deformation density calculated by using the phases from the spherical atom structure factor calculation. [b] Electron deformation density calculated by using the phases from the multipole refinement structure factor calculation.

density distribution in the N–HN···Cl hydrogen bond and in the O1–HO1···Cl hydrogen bond. (The hydrogen bonds are indicated by dashed lines.) One should notice that there is no electron density in the center of the hydrogen bonds, as expected, since the formation of these types of interactions are a result primarily of electrostatic attractions with little covalent contribution. The chloride ion shows an approximately spherical distribution of density which corresponds to the negative charge on the ion, −0.65 (13). The contours in the center of the chloride ion are actually decreasing in height to form a slight depression at the atom center.

Since the space group of naloxone hydrochloride dihydrate is acentric, only the amplitude, and not the phase, of the structure factor, F_o, can be determined from the experiment. When a fit of the density has been obtained by a multipole deformation refinement, the phases calculated in the refinement can be used to calculate a properly phased model deformation density. It has been estimated that phases of ΔF distributed at random will result in a reduction in the size of the features in the deformation density by a factor between 0.5 and 1.0.[12] In an effort to quantify the effect of using phases calcualted in the multipole refinement versus the conventional method using phases from a spherical atom refinement, both types of deformation density maps were calculated for each plane shown in the composite maps in Figures 3 and 4. An example is shown in Figure 7.

Figure 7a shows a model deformation density map calculated by using only the phases obtained from a conventional spherical atom refinement. Figure 7b shows a model deformation density map calculated by using the phases from the multipole model refinement. It is apparent that a proper treatment of the phases

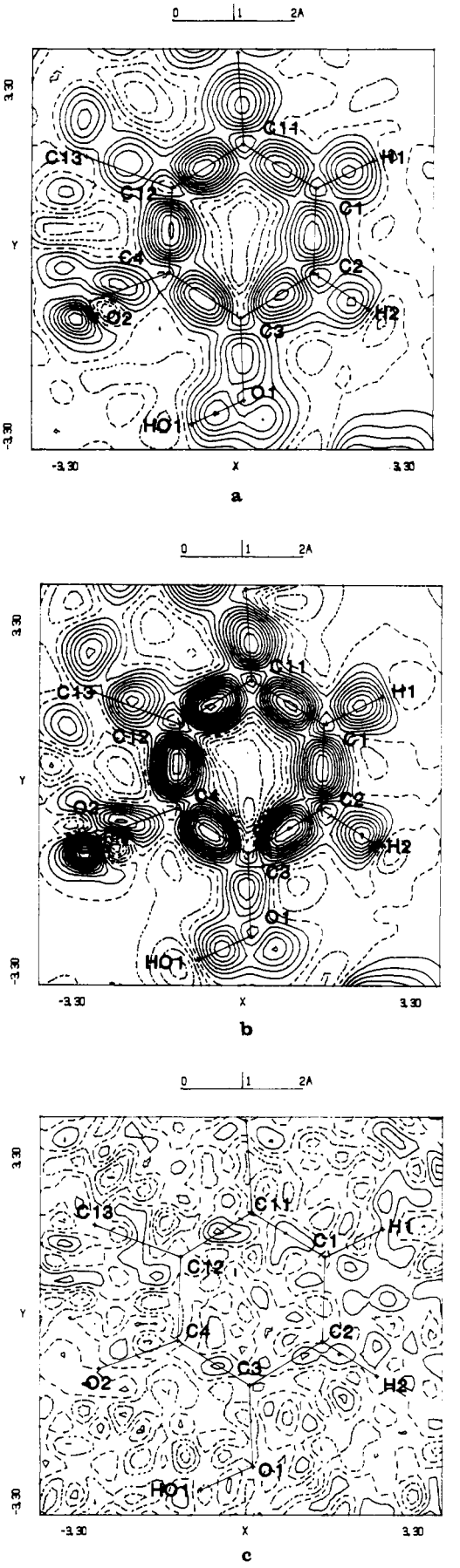

Figure 7. Electron deformation density plotted in the aromatic ring calculated by using phases from (a) the spherical atom refinement model, and (b) the multipole refinement model. (c) Residual density plotted in the same plane. Contours of all maps plotted as in Figure 4.

can result in a deformation density map with sharper, more distinct density features. Table IV has a list of all bond types in naloxone hydrochloride dihydrate and the effect that the treatment of phase has on the density in each bond type. In all bond types not involving oxygen atoms, the effect of not using the phase calculated in the multipole refinement is to reduce the size of the features in the deformation density by a factor of 0.68–0.70. The C–O bonds show density that is much more diffuse and lower in height than other bonds for reasons described above. Adjusting the phases does not seem to have the same effect on the density features in these bonds as it does on better defined density features.

Figure 7c shows the residual density plotted in the aromatic ring plane. There appear to be no significant areas of electron density not fit by the model. The largest peak is 0.15e Å^{-3} compared with an estimated standard deviation of 0.05e Å^{-3}. The monopole population parameters, listed in Table III, were obtained from refinement IV described above. Values of P_v give the population of electrons in a function centered on each atom used to define the spherical features of the electron density. In this type of refinement, the values obtained for P_v can be used to calculate the net atomic charges on each atom with the same reliability as the net atomic charges obtained in sophisticated theoretical calculations (Net atomic charge (q) = number of valence electrons – P_v). However, caution must be exercised in interpreting these net atomic charges. The least-squares program used to refine these multipole population parameters uses continuous functions to define the electron density on each atom. The problem of where to partition the density functions for each atom arises, and the absolute values for the net atomic charges calculated from the monopole populations may or may not be significant. However, areas in the deformation density map show more electron density contours than other areas in the map can be believed to be electron rich. The difference is that the electron density of an atom is a real, measurable physical property and the net atomic charge is a defined property which depends on the partitioning method.

In naloxone hydrochloride, the net atomic charge on each atom does not appear to give consistent information concerning areas of the molecule that are electron rich or electron deficient with the exception of the oxygen atoms and the nitrogen atom, which appear to be electron rich (all have negative net atomic charges). If, in fact, the net atomic charge depends on the method of partitioning the density functions, then it seems reasonable to consider the total charge in a particular area of the molecule by defining a "local area charge". For example, the charge in the area near a hydroxide oxygen atom also depends on the net atomic charge of the atoms to which it is bonded. The net atomic charge for O1 is –0.49. The local area charge of O1 would be the sum of the net atomic charges for O1 and the atoms to which it is bonded ($q_{O1} + q_{C3} + q_{HO1}$ = (–0.49) + (+0.09) + (+0.60) = + 0.20). Figure 8 shows a diagram of the two faces of the molecule. The number next to each atom is the local area charge for that atom. These local area charges have been useful in establishing trends of charge through certain areas of the molecule. The fused atoms in the aromatic ring tend to be more negative than the peripheral atoms. (This phenomenon has been observed in the electron density distribution of carcinogenic polyaromatic hydrocarbons.[20]) Additionally, the charge on the molecule appears to become more negative in the region around the hydroxide group bonded to C14 and in the region around the nitrogen atom. In fact, this region of naloxone hydrochloride dihydrate has the most negative local area charges in the molecule. Interestingly, the OH group bonded to the aromatic ring (as well as the ketone oxygen) does not appear to be significantly charged. The *N*-allyl substituent becomes more positive on the atoms farther away from the nitrogen atom. Again, one must refrain from assigning too much physical significance to the individual atomic charges. However, it is useful to point out that very similar (although not identical) trends have been observed in the local area charges calculated from X-ray data on morphine free base.[22]

(22) Pant, A. K.; Stevens, E. D.; Klein, C. L., unpublished results.

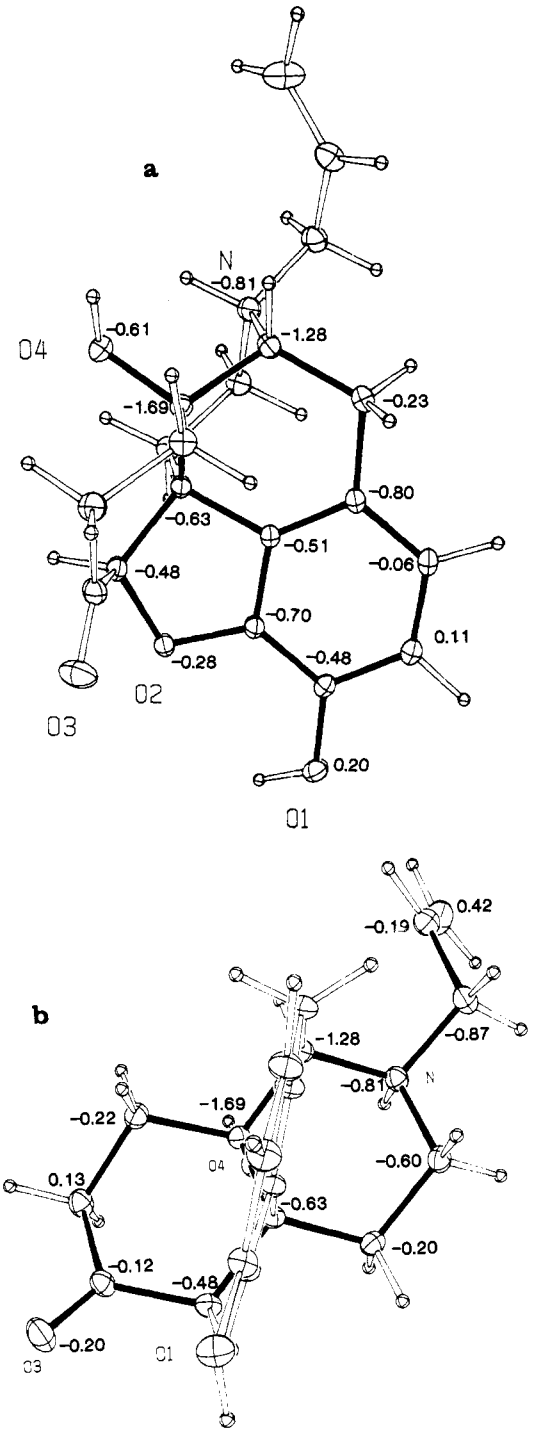

Figure 8. Distribution of "local area charges" for the two faces of naloxone.

The dipole moment of the naloxone molecule, relative to the center of mass of the molecule, is calculated to be 53 (5) D by integration over the multipole deformation functions.

Discussion

A common structural feature of opiates and other drugs active at the opiate receptor is a tertiary amine nitrogen, usually incorporated in a piperidine ring. This suggests a significant role for the amine nitrogen in binding to the receptor. At physiological pH, these molecules are presumed to exist in the N-protonated form. Thus, most models for the receptor include an "anionic" site to which the protonated nitrogen binds.[23-25]

(23) Beckett, A. H.; Casey, A. F. *J. Pharm. Pharmacol.* **1954**, *6*, 986–1001.

Since the presence of an OH group at C14 appears to increase antagonist activity (naloxone vs oxymorphone and nalorphine vs morphine), a common anionic receptor has been postulated to interact with both the protonated nitrogen and the OH group.[26] In contradiction to this model, substitution of alkoxy groups for the OH group does not lower antagonist activity.[27] It is also reported that N-methylated quaternary derivatives of naloxone still show some antagonist activity.[28]

Clearly, any model for the receptor must accommodate the distribution of charge and hydrogen bond donors and acceptors in the drug molecules. Molecular orbital calculations may be used to obtain approximate distributions of atomic charges in such molecules. Numerous theoretical calculations of opiates and related molecules have been performed[26,29-31] with gradually improving methods. More recent calculations have investigated electrostatic potentials and donor–acceptor properties of the molecular orbitals.[32]

Perhaps the most remarkable result of the X-ray experiment is the net negative charge on the nitrogen atom. That this result is not due to a partitioning problem is evident from the local area charge calculated for the nitrogen atom, which is even more negative. The result is also consistent with preliminary high-resolution measurements of the charge on the protonated nitrogen of methadone hydrochlorides[33] and of the unprotonated nitrogen of morphine,[22] which both yield similar negative values. Previous theoretical calculations have indicated that the positive charge is delocalized over the molecule, rather than localized on the nitrogen, as the formal charge would imply.[29] It is possible that some of the negative charge on the nitrogen may be attributed to a partial neutralization of charge on the chloride ion through the N–H···Cl hydrogen bond. The charge on the chloride ion is reduced from its formal value of −1.00 to an observed value of 0.65 (13).

Although theoretical charges are not directly comparable to values derived from the X-ray experiment because of the difference in the method by which the charge is obtained, the experimental charges are generally in good agreement with charges calculated for both protonated and unprotonated morphine and nalorphine at chemically equivalent atoms other than in the region of the nitrogen atom. Charges from ab initio calculations[31] are in somewhat better agreement with the experiment than those from various semiempirical methods.[29,30]

If further studies of related molecules in progress reveal the negative charge on the protonated nitrogen to be a common feature of these molecules, then clearly a careful reexamination of the standard model for the receptor in which the cationic head of the drug molecule is bound by ionic forces to an anionic site on the receptor is necessary. A reasonable alternative description of the role of the nitrogen is simply as a hydrogen bond donor. Similarly, the OH group on C14 may simply act as a hydrogen bond acceptor to the antagonist form of the receptor. The experimental electron distribution of naloxone hydrochloride will be used to calculate the experimental electrostatic potential, which, being a well-defined molecular property, should provide additional information on the electrostatic characteristics of interaction with various receptor models.

Conclusion

The successful mapping of the electron density distribution in naloxone hydrochloride demonstrates that accurate information on the electronic structures of moderately large molecules may be obtained from high-resolution X-ray diffraction experiments. The estimated error in the deformation density is remarkably small, 0.05 e $Å^{-3}$, and comparable to that in current studies on small molecules. To achieve similar accuracy from theoretical calculations would require an ab initio calculation with an extended basis set including polarization functions.

As expected for an acentric structure, considerable enhancement of the features of the deformation density is observed when structure factor phases obtained from a multipole refinement model are used. Subtle features of the bonding such as "lone pair" density on the oxygens and elongation of the bond peaks out of the plane in the allyl double bond are clearly visible in the deformation density. Atomic charges, a property not rigorously defined but chemically useful, are in reasonable agreement with approximate theoretical calculations. However, a negative charge is observed on the protonated nitrogen, casting doubt on models for the drug–receptor interactions, which include "ionic bonding" between the cationic head of the drug and an anionic site on the receptor.

Acknowledgment. Support of this work by the National Institutes of Health (Grant NS-19789) is gratefully acknowledged.

Registry No. 2, 465-65-6; **2**·HCl·$2H_2O$, 51481-60-8.

Supplementary Material Available: Tables of atomic coordinates, anisotropic thermal parameters for non-hydrogen atoms, bond lengths and bond angles, and refined multipole populations and radial parameters for naloxone hydrochloride (9 pages); observed and calculated structure factor amplitudes for naloxone hydrochloride (51 pages). Ordering information is given on any current masthead page.

(24) Portoghese, P. S. *J. Pharm. Sci.* **1966**, *55*, 865–887.
(25) Feinberg, A. P.; Creese, I.; Snyder, S. H. *Proc. Natl. Acad. Sci. U.S.A.* **1976**, *73*, 4215–4219.
(26) Loew, G. H.; Berkowitz, D. S. In *Opiates and Endogenous Opioid Peptides*; Elsevier: Amsterdam, 1976; p 387.
(27) Kobylecki, R. J.; Carling, R. W.; Lord, J. A. H.; Smith, C. F. C.; Lane, C. C. *J. Med. Chem.* **1982**, *25*, 116–120.
(28) Schulz, R.; Wuster, M.; Herz, A. *Naunyn-Schmiedebergs Arch. Pharamakol.* **1979**, *308*, 255.
(29) Kaufman, J. J.; Kerman, E.; Koski, W. S. *Int. J. Quantum Chem., Quantum Biol. Symp.* **1974**, *No. 1*, 289–313.
(30) Lowe, G. H.; Berkowitz, D. S. *J. Med. Chem.* **1975**, *18*, 656–662. Lowe, G. H.; Berkowitz, D. S. *Ibid.* **1978**, *21*, 101–106. Popkie, H. E.; Koski, W. S.; Kaufman, J. J. *J. Am. Chem. Soc.* **1976**, *98*, 1342–1345.
(31) Cheney, V. B.; Zichi, D. A. *Int. J. Quantum Chem., Quantum Biol. Symp.* **1981**, *No. 8*, 201–219.
(32) Majeste, R. J.; Stevens, E. D.; Klein, C. L., unpublished results.